Widespread white matter and conduction defects in *PSEN1*-related spastic paraparesis

Steffan K. Soosman, B.S.[a], **Nelly Joseph-Mathurin, Ph.D.**[b], **Meredith N. Braskie, Ph.D.**[c], **Yvette M. Bordelon, M.D., Ph.D.**[d], **David Wharton, B.S.**[d,e], **Maria Casado, B.A.**[d,e], **Giovanni Coppola, M.D.**[f], **Holly McCallum, M.D.**[c], **Marc Nuwer, M.D., Ph.D.**[e], **Pedro Coutin-Churchman, M.D., Ph.D.**[e], **Liana G. Apostolova, M.D., M.S.**[d,e,g], **Tammie Benzinger, M.D.**[b], and **John M. Ringman, M.D., M.S.**[c,d,e]

Steffan K. Soosman: ssoosman@hawaii.edu; Nelly Joseph-Mathurin: n.joseph@wustl.edu; Meredith N. Braskie: Meredith.Braskie@ini.usc.edu; Yvette M. Bordelon: YBordelon@mednet.ucla.edu; David Wharton: david.m.wharton@vanderbilt.edu; Maria Casado: MCasado@mednet.ucla.edu; Giovanni Coppola: gcoppola@ucla.edu; Holly McCallum: holly.maccallum@gmail.com; Marc Nuwer: MNuwer@mednet.ucla.edu; Pedro Coutin-Churchman: PChurchman@mednet.ucla.edu; Liana G. Apostolova: lapostol@iu.edu; Tammie Benzinger: benzingert@wustl.edu

[a]University of Hawaii, John A. Burns School of Medicine, 651 Ilalo Street Honolulu, HI 96813, Honolulu, HI

[b]Mallinckrodt Institute of Radiology, Washington University School of Medicine in St. Louis, Campus Box 8131, 510 South Kingshighway Boulevard, St. Louis, MO 63110

[c]Department of Neurology, Keck School of Medicine of USC Center for the Health Professionals, 1540 Alcazar Street, Los Angeles, CA, 90089

[d]Department of Neurology, David Geffen School of Medicine at UCLA, 710 Westwood Plaza, Los Angeles, CA, 90095

[e]Mary S. Easton Center for Alzheimer's Disease Research, David Geffen School of Medicine at UCLA, 710 Westwood Plaza, Los Angeles, CA, 90095

[f]Semel Institute for Neuroscience and Human Behavior, Departments of Psychiatry & Neurology, David Geffen School of Medicine, #3506C Gonda Neuroscience and Genetics Research Center, UCLA, 695 Charles E. Young Dr. South, Los Angeles, CA 90095

[g]Indiana University School of Medicine, Indiana Alzheimer's Disease Center, 355 W 16th Street, Suite 4700, Indianapolis, IN 46202

Corresponding Author: John M. Ringman M.D., M.S., Professor of Clinical Neurology, Department of Neurology, Keck School of Medicine of USC, Center for the Health Professionals, 1540 Alcazar Street, Suite 209F, Los Angeles, CA 90089-0080, (323) 442-0321, john.ringman@med.usc.edu.

Abstract

The mechanisms underlying *PSEN1* mutation-associated spastic paraparesis (SP) are not clear. We compared diffusion and volumetric magnetic resonance measures between 3 persons with SP associated with the A431E mutation and 7 symptomatic persons with *PSEN1* mutations without SP matched for symptom duration. We performed amyloid imaging and central motor and somatosensory conduction studies in one subject with SP. We found decreases in fractional anisotropy and increases in mean diffusivity in widespread white matter areas including the corpus callosum, occipital, parietal, and frontal lobes in *PSEN1* mutation carriers with SP. Volumetric measures were not different and amyloid imaging showed low signal in sensorimotor cortex and other areas in a single subject with SP. Electrophysiological studies demonstrated both slowed motor and sensory conduction in the lower extremities in this same subject. Our results suggest that SP in carriers of the A431E *PSEN1* mutation is a manifestation of widespread white matter abnormalities not confined to the corticospinal tract that is at most indirectly related to the mutation's effect on APP processing and amyloid deposition.

Keywords

PSEN1; spastic paraparesis; white matter; diffusion tensor imaging; electrophysiology

1. Introduction

Alzheimer's disease (AD) is the most common cause of neurodegenerative dementia and an estimated 5.3 million Americans are currently afflicted by it(Alzheimer's, 2015). Of these persons, an estimated 200,000 are below aged 65(Alzheimer's, 2015) and a subset of these have autosomal dominant AD (ADAD). ADAD is an early onset form of AD caused by the presence of essentially fully-penetrant mutations in one of three genes; Presenilin 1 (*PSEN1*), Presenilin 2 (*PSEN2*) or Amyloid Precursor Protein (*APP*). The observation that pathogenic mutations in these genes affect cleavage of APP(Scheuner et al, 1996) is supportive evidence for a pivotal role of the β-amyloid (Aβ) protein in the etiology of AD(Hardy and Selkoe, 2002). Though increased relative or absolute production of the 42-amino acid length version of Aβ (Aβ42) has been reproducibly demonstrated in ADAD(Ringman et al, 2008), such overproduction is less evident in late-onset AD (LOAD). The prevailing hypothesis for the development of LOAD is a diminished ability to eliminate Aβ, leading to its aggregation and deposition(Tanzi et al, 2004). Despite this apparent difference, both LOAD and ADAD share pathological features including neurofibrillary tangles(Ringman et al, 2016) and most often present with memory and executive deficits as well as personality changes(Ringman et al, 2011; Ringman et al, 2015). However, a significant subset of persons with ADAD, particularly when due to *PSEN1* mutations, can have features atypical for AD including early myoclonus, pseudobulbar affect, and gait abnormalities due to spastic paraparesis (SP)(Joshi et al, 2012). SP can be the initial symptom, occur concurrently with, or somewhat after cognitive and behavioral changes in *PSEN1*-related ADAD and occurs in association with specific mutations(Karlstrom et al, 2008; Larner, 2013). The pathologic basis of SP and other clinical variants in *PSEN1*-related AD is controversial(Rudzinski et al, 2008; Yokota et al, 2003) and it is unclear whether it is

related to qualitative or quantitative differences in APP processing, differences in the localization of resulting pathology(Martikainen et al, 2010), or other effects of *PSEN1* mutations(Xia et al, 2015).

The development of diffusion-weighted (DWI) magnetic resonance imaging (MRI) has allowed for sensitive delineation of white matter pathology *in vivo* (Bozzali et al, 2002; Medina et al, 2006). DWI measures both the direction and magnitude of proton diffusion. Such diffusion can be characterized by overall magnitude (mean diffusivity or MD) and tendency for the diffusion to be directionally dependent. Diffusion direction can be characterized by fractional anisotropy (FA): an index of the tendency of water to diffuse in a single direction obtained by calculating a diffusion tensor for each voxel (i.e. diffusion tensor imaging or DTI). Proton diffusion in white matter is typically parallel to fiber tracts and therefore FA and other DTI indices provide measures of white matter integrity(Ringman et al, 2007) and may distinguish demyelinating from degenerative processes(Song et al, 2003). DTI can help delineate anatomical white matter changes but SP in *PSEN1*-related AD, has not been well described electrophysiologically. Such characterization can help delineate the nature and extent of white matter tract involvement.

Through the development of ligands that bind relatively selectively to fibrillar amyloid and can be radioactively labeled to allow detection using positron emission tomography ("amyloid PET"), we can now identify and localize amyloid deposition during life(Klunk et al, 2003). The relationship between the distribution of such pathology to defined anatomical pathways can help elucidate the role amyloid plaques play in symptom manifestation. In the current paper we sought to comprehensively assess the MRI characteristics of white matter involvement in SP in 3 carriers of the A431E *PSEN1* mutation relative to 7 persons symptomatic from *PSEN1* mutations but without SP. Furthermore, we performed additional assessments with amyloid PET using Pittsburgh Compound B (PiB) and motor and somatosensory evoked potential studies in one A431E *PSEN1* mutation carrier with SP.

2. Methods

2.1 Subjects

Subjects or their surrogates gave written informed consent as part of an IRB-approved observational study of ADAD at UCLA. The ten subjects that were included were symptomatic from known pathogenic *PSEN1* mutations, were aware of their mutation status, and had DTI available. Subjects underwent comprehensive clinical evaluations including the Mini-Mental Status Examination(Folstein et al, 1975) and Clinical Dementia Rating scale(Morris, 1997). The CDR is a global scale of dementia severity based on an interview with the subject and a knowledgeable informant. A score of 0 represents normalcy, 0.5 indicates questionable or mild impairment, 1 mild, 2 moderate, and 3 severe dementia. The subjects were defined as having SP if leg spasticity interfered with their ability to ambulate before or within two years of the onset of cognitive symptoms. Time since onset of cognitive or motor symptoms was quantified in years. Subjects also underwent *APOE* genotyping using standard techniques.

2.2 Image Acquisition

All subjects underwent structural T1-weighted MRI scans and DTI. All subjects but one (without SP) underwent Susceptibility Weighted Imaging (SWI) or T2-star weighted (T2*) MR from which microhemorrhage (MCH) count could be evaluated. Eight subjects underwent fluid attenuated inversion recovery (FLAIR) MRI sequences (3 with SP and 5 without) and 5 subjects had a PiB PET scan (one with SP and 4 without).

All MR images were obtained on the same 3T Siemens Trio Scanner using a 32-channel phased array head-coil. The DTI protocol has been previously described(Ryan et al, 2013) and consisted of 64 gradient directions acquired via a single-shot spin-echo echo planar imaging (EPI) sequence (FOV 240 mm, matrix 96x96, yielding an isotropic voxel of $2.5x2.5x2.5mm^3$ and 55 contiguous axial slices, TR=6800ms, TE=91ms, b-value=1000s/mm^2, augmented with parallel imaging acceleration (GRAPPA)). Nine acquisitions without diffusion weighting (b=0s/mm^2) were also acquired.

All subjects also underwent volumetric structural T1 weighted imaging using MPRAGE, obtained in the sagittal plane (TR=2300ms, TE=2.95ms, voxel resolution=$1.1x1.1x1.2mm^3$). To evaluate for the presence of MCHs, 6 subjects underwent SWI in the axial plane (TR=28ms, TE=20ms, voxel resolution=$0.7x0.7x2.4mm^3$) and 3 underwent T2* in the axial plane (TR=650ms, TE=20ms, voxel resolution=$0.8x0.8x4mm^3$). To evaluate for the presence and extent of white matter hyperintensities (WMH), 8 subjects underwent axial T2 weighted FLAIR MRI imaging (TR=9000ms, TE=90ms, voxel resolution=$0.9x0.9x5.0mm^3$).

Five subjects also underwent a PiB scan (one with SP, "AJ", and 4 without). PiB imaging was performed with a bolus injection of approximately 15 mCi of $[^{11}C]$PiB. Dynamic acquisition consisted of either a 70-minute scan starting at injection or a 30-minute scan beginning 40 minutes post-injection.

2.3 Image processing and analysis of DTI data

DTI processing was performed using the Diffusion Weighted Imaging Toolbox in FSL (http://www.fmrib.ox.ac.uk/fsl/). Prior to processing, the two diffusion sequences were averaged and then concatenated with the 9 B0 acquisitions to create a single 4D volume for processing. For one subject without SP, only one DTI volume was acquired. Volumes were subjected to eddy current correction and linear realignment to the first image. Diffusion tensors were then calculated after applying a brain mask generated from FSL's Brain Extraction Tool. The resulting Fractional Anisotropy (FA), Mean Diffusivity (MD), axial diffusivity (AD) and radial diffusivity (RD) maps were used for analysis. Conversion of all outputs to standard space was achieved via FSL's Tract Based Spatial Statistics (TBSS) toolbox, which performed nonlinear registration to FSL's FA template map followed by a sequential nonlinear and affine transformation into MNI space. The processed FA images were then combined to generate a mean FA image for the group, which was used to create a mean FA "skeleton" to limit voxel statistics to white matter. A threshold of 0.20 was used to include white matter (WM) tracts that were both common to all subjects and the most aligned, while excluding potential non-WM regions. Individual subject FA images were then projected onto this skeleton to create skeletonized FA images for statistical analysis.

2.4 Volumetric analyses

The MPRAGE images of all subjects were registered in the same space and automatically segmented to obtain cortical reconstruction and volumetric segmentation using FreeSurfer v5.1 (http://surfer.nmr.mgh.harvard.edu/). Visual inspection of the automated segmentation was done for quality control. Eleven regions of interest (ROIs) were selected. The cortical thicknesses of the frontal, parietal, temporal, and occipital lobes, and the volume of the cerebellum, hippocampus (left and right), caudate, putamen, pallidum, and amygdala of each subject were normalized by their intracranial volume and used for structural and atrophy analyses.

2.5 Microhemorrhage count

The number of MCH on SWI and T2* images were manually counted by author N J-M and reviewed and confirmed by author TB.

2.6 White Matter Hyperintensities

The degree of periventricular white matter hyperintensity (WMH) was scored on FLAIR images by author N J-M and confirmed by author TB using Fazekas' scale(Fazekas et al, 1987). Quantification of WMH volume was performed using a Matlab/SPM tool developed in house at Washington University. Briefly, the volume of voxels with an intensity above a specified threshold in segmented white matter volumes from FLAIR images were totaled.

2.7 PiB PET analyses

C^{11}-PIB PET images were analyzed using NeuroQ (Syntermed Inc, Atlanta, www.syntermed.com). After correction for tissue-based attenuation NeuroQ implements an algorithm for automatically measuring the number of radioactive events emitted by a positron source per second from pixel locations assigned by a computerized reconstruction algorithm as falling within 240 standardized planar regions of interest (ROI) defined on each transaxial plane of the PET scan. These regions were defined after each PET scan was transformed to the NeuroQ template space. The 240 NeuroQ transaxial regions are then automatically grouped into 47 3D standardized volumes of interest (sVOI) corresponding to distinct neuroanatomical (e.g. left inferior parietal lobule) or functional areas (e.g., Broca's area) as previously described(Torosyan and Silverman, 2012). All mean activity values are automatically normalized to the mean pixel activity measured in the cerebellar cortex producing standard uptake volume ratio (SUVR) units.

2.8 Electrophysiological Measures

Electrophysiological measures were also performed on subject AJ. Central motor conduction time (CMCT) was computed by establishing the total M-wave latency by stimulating the left motor cortex while recording the latency of a motor evoked potential (MEP) in the right first dorsal interosseous muscles (FDI) and tibialis anterior muscle. F-wave latency to these muscles was then calculated and half this latency was subtracted from the M-wave latency to determine the CMCT. Somatosensory evoked potentials (SSEPs) from the right arm and leg were assessed by stimulating the median nerve at the wrist and the posterior tibial nerve at the ankle. Upper limb SSEPs were recorded from the ipsilateral Erb's point (N9), over the

fifth cervical spinal process and contralateral parietal scalp (N20). Lower limb SSEPs were recorded from the ipsilateral popliteal fossa (N8) and scalp (P37). CMCT and SSEP latencies on the index patient were compared against gender and height matched laboratory standards.

2.9 Statistical analysis

All of the imaging analyses described above were performed blind to the presence of SP. Comparisons of demographic variables and quantitative and semi-quantitative imaging variables were then made between subjects with and without SP using two-tailed chi square tests (and Fisher's exact tests when appropriate) and Mann-Whitney U tests for categorical and ordinal/numerical variables using SPSS (version 23).

For DTI, voxel-wise statistical analyses were performed via a permutation-based inference randomized program in FSL to compare differences between subjects with and without SP. The threshold of the resulting statistical maps was set to $p < 0.05$ corrected at the cluster level for multiple comparisons using False Discovery Rate (FDR).

For PIB analyses, mean SUVR was computed using the Clark method(Clark, Schneider, 2011). SUVR's were compared in all regions between the one subject with SP (subject AJ) and 4 without by Mann-Whitney U tests.

3 Results

3.1 Subjects

Ten subjects affected by pathogenic *PSEN1* mutations were studied, including 3 with SP and 7 without (see Table 1 for demographics and clinical information). All 3 subjects with SP were unable to walk independently whereas none of the 7 non-SP subjects had any difficulties with ambulation. All ten had cognitive symptoms with 5 having CDR scores of 0.5 (2 with SP, 3 without), 2 w/CDR scores of 1 (both without SP, 1 w/CDR score of 2 (no SP), and 2 w/CDR scores of 3 (one with and one without SP). All three subjects with SP were males with the A431E *PSEN1*(Murrell et al, 2006; Yescas et al, 2006) mutation while the 7 without SP were more diverse with regards to gender (5 were female) and mutation (1 with the A431E, 2 with the G206A(Athan et al, 2001), and one each with the R269H(Gomez-Isla et al, 1997), S212Y(Ringman, Gylys, 2011), I238M(Ting et al, 2014), and M146L(Morelli et al, 1998) *PSEN1* mutations). Subjects with and without SP were comparable with regards to mean age (48.7 vs. 54.7), disease duration (5.3 years), MMSE (15.3 vs. 18.0), and CDR sum of boxes score (6.7 vs. 6.9). Notably, 2 of the 3 subjects with SP were of the *APOE* ε3/4 genotypes and the remaining subject with SP had the *APOE* ε2/3 genotype. Six of the seven subjects without SP had the *APOE* ε3/3 genotype with the remaining subject having the *APOE* ε4/4 genotype.

3.2 DTI Results

Relative to those without SP, decreased FA was seen in subjects with SP in widespread areas of white matter including in the corpus callosum, occipital, parietal, and frontal lobes. It extended into the corona radiata and centrum semiovale and also into the precentral gyri

among other gyri bilaterally (Figure 1A). Increased MD was also seen in comparable areas except with extension into the right temporal lobe (Figure 1B). Comparison of axial (L1) diffusivity did not demonstrate any differences between persons with and without SP while radial diffusivity (L2 & L3) was increased in persons with SP in areas overlapping those of FA decrease (Figure 1C).

3.3 White Matter Hyperintensities

The volume of WMH and Fazekas score did not differ between those with and without SP (Table 2). However, it is noteworthy that all the SP participants presented a Fazekas' score above 0 and a volume of WMH >10,000mm^3, thus abnormal white matter readily visible on MRI. Interestingly, the variability in the extended volume of WMH in the SP group (n=3) was low, while the non SP group (n=5) displayed more variability. The non SP group presented only one subject with a volume of WMH > 10,000mm^3 and 2 subjects with normal WM assessed by Fazekas' score.

3.4 Volumetric analyses

There were no statistically significant differences in the volumes of any cerebral structures (cerebellum, caudate, putamen, pallidum, amygdala, hippocampi) or cortical thickness in any region (temporal, frontal, parietal, or occipital) between persons with and without SP though the means of all such measures were numerically lower in persons with SP (Table 2).

3.5 Microhemorrhage count

MCH count was available for all 3 subjects with SP and on 6/7 of those without SP. Number of MCHs was not statistically different between groups. Notably, however, 2 of the 3 persons with SP had MCH counts of greater than 100 (see Figure 2) while only one of the 6 subjects without SP had MCHs (n = 73) (Table 2).

3.6 PiB PET

PiB PET was available and analyzed for 4 persons without SP and one subject with SP (AJ). There were no areas of significantly different SUVR between AJ and the 4 without SP including in the sensorimotor cortices and basal ganglia (see table 3 for representative areas, Figure 3) though AJ had the numerically lowest mean cortical binding potential (0.21 relative to a mean of 0.84, range from 0.24 – 1.18, threshold for positivity = 0.18, Figure 3). SUVR for the left and right sensorimotor cortices were 1.15 and 1.06 in AJ (means SUVRs in these areas for the 4 subjects without SP, 1.97 and 1.99, respectively). AJ had relatively selective increased amyloid signal in the thalami but this was not significantly different from those without SP.

3.7 Electrophysiological Studies

In AJ, CMCT of the right lower extremity was markedly slow with a latency of 34.8 ms, (normal < 16.5 ms) while that of the right upper extremity was normal at 8.2 ms (normal < 9.7 ms). SSEPs were mildly slowed in the lower (N8 - P37 latency 39.1 ms, normal < 36.0 ms) but not upper extremities N9 - N20 = 9.7 ms, normal < 10.6 ms).

4 Discussion

In this study, we performed comprehensive characterization of *PSEN1* mutation carriers with and without SP in an attempt to elucidate the underlying pathophysiology. We found robust and widespread decreases in white matter integrity as indexed by decreased FA, increased MD, and apparent length-dependent slowed central conduction times including SSEPs. FA decreases and MD increases were seen in white matter underlying motor cortex consistent with the conduction abnormalities observed. These findings in the context of relatively preserved gray matter volumes and lack of amyloid deposition in sensorimotor cortex in one subject are supportive of an effect of the A431E *PSEN1* mutation on white matter in part independent of APP mismetabolism.

Previous studies regarding the pathology associated with *PSEN1*-related SP are limited. There is a frequent, though not invariable(Kwok et al, 1997; Shrimpton et al, 2007), association between SP and atypical "cotton-wool" amyloid plaques ("CWP") demonstrated on neuropathologic examination(Houlden et al, 2000) and CWPs are present in persons dying with the A431E *PSEN1* mutation(Roher et al, 2013). CWPs are large amyloid plaques lacking neuritic cores that consist largely of Aβ42 species truncated near the amino terminal(Miravalle et al, 2005). Though occasionally reported in LOAD(Le et al, 2001) they are most frequently associated with *PSEN1* mutations that cause extremely high levels of Aβ42 to be produced(Houlden, Baker, 2000; Karlstrom, Brooks, 2008), suggesting the possibility of qualitative or quantitative differences in APP processing in their genesis. In light of the variable co-occurrence of SP and CWPs(Yokota, Terada, 2003) however, the mechanism through which they are linked is unclear. Verkkoniemi et al(Verkkoniemi et al, 2001) found abundant CWPs in medial primary motor cortex associated with degeneration of the lateral corticospinal tract, suggesting a cause-and-effect relationship. Rudzinski et al similarly observed degeneration of the corticospinal tracts with sparing of the medial lemniscus in a patient with SP and a *PSEN1* mutation but did not find disproportionate involvement of the motor cortex with AD pathology(Rudzinski, Fletcher, 2008). The lack of significant PiB signal in the sensorimotor cortex in the one patient in our study with SP assessed using this modality argues against fibrillar amyloid plaques playing a direct role in the development of this corticospinal sign. A previous PiB study in "variant" *PSEN1*-related AD with SP similarly failed to find excessive amyloid deposition in sensorimotor cortex but did find disproportionate deposition in the striatum(Koivunen et al, 2008) as did a recent study of a single subject with SP(Lyoo et al, 2016). Importantly, tau PET imaging using ^{18}F-AV-1451 was performed in this latter study which revealed increased signal in sensorimotor cortex, particularly contralateral to the hemibody which was most affected by spasticity. Tau deposition was higher in widespread areas of cortex relative to controls with LOAD including in medial and lateral parietal lobes, inferior temporal lobes, and occipital lobes. This is consistent with cortical neurofibrillary pathology being a correlate, and potentially causative, of the white matter pathology we identified with DTI. It should be noted however, that PiB does not bind equally to all forms of amyloid plaques(Ringman et al, 2012), and the nature of its binding to the CWPs frequently present in *PSEN1*-related SP has not to our knowledge been well characterized.

O'Riordan et al described SP in *PSEN1*-related AD associated with extensive cerebral amyloid angiopathy (CAA) and white matter changes presumably of ischemic origin and suggested a causal relationship(O'Riordan et al, 2002). MCHs were extensive in two of the three subjects with SP in our study and interestingly, these two had the *APOE* ε2/3 and 3/4 genotypes with the remaining subject with SP having the 3/4 genotype as well. An association of diffusely diminished FA with lobar MCHs in *APOE* ε4 carriers has been reported and was interpreted as the MCHs representing the "tip of the iceberg" with regards to more subtle and diffuse affectation of white matter(Akoudad et al, 2013). The relationship of MCHs with SP is not clear however, as not all subjects with SP have MCHs and clearly non-ADAD patients with CAA and MCHs do not typically develop SP. MCHs do not appear to explain our DTI findings in that two of the subjects in the current study were siblings of whom one had SP and no MCHs (*APOE* ε3/4) while the other (*APOE* ε3/3) had 73 MCHs but no SP. The subject with MCHs but without SP had numerically "more normal" DTI indices. In addition, how MCHs would give rise to the SSEPs abnormalities (see below) is unclear. We hypothesize that any relationship of MCHs and *APOE* genotype with SP is an indirect one though further studies are required to better define this.

We found increased MD in persons with SP in a pattern similar to, but to a greater extent than that of decreased FA. In a prior study of seven presymptomatic ADAD mutation carriers investigators found increases in MD but not FA, suggesting changes in mean diffusivity may be a more sensitive measure of white matter changes in this population(Li et al, 2015). When axial and radial diffusivity were separately compared between persons with and without SP, we found increased radial diffusivity in persons with SP in a pattern similar to the FA differences but no differences in axial diffusivity. Increased radial diffusivity has been interpreted to represent pathology of myelin rather than axons(Song, Sun, 2003; Song et al, 2002). The pathology underying DTI changes in AD is unclear, with reports of both increased radial and axial diffusivity(Back et al, 2011; Sun et al, 2014). Though loss of corticospinal projection neurons (Betz cells) as reflected in the neurofibrillary pathology in motor cotex seen in the study by Lyoo et al(Lyoo, Cho, 2016) might account for the spastic paraparesis, a direct effect of the A431E mutation on myelin cannot be ruled out. Such a direct effect in carriers of *PSEN1* mutations is suggested by a gene expression study in which mRNA for Presenilin-1 was highly co-expressed with myelin proteins(Miller et al, 2008). However, *PSEN1* mutations might also lead to white matter abnormalities and SP through other effects on axons and axonal transport as evidenced in studies of transgenic animals(Pigino et al, 2003; Wirths et al, 2006). Persons with *PSEN1* mutations, including the A431E mutation and others giving rise to spastic paraparesis, have been shown to have biochemical abnormalities in white matter distinct from that of late-onset AD(Roher, Maarouf, 2013).

We previously reported substantially diminished FA in a cohort of presymptomatic persons with ADAD mutations (Ringman, O'Neill, 2007). Though those findings appeared robust, such differences are not always found during the presymptomatic phase of the autosomal dominant AD (Sanchez-Valle et al, 2016). Notably, only one of the nine mutations studied in that report has been described as being associated with SP(Karlstrom, Brooks, 2008; Llado et al, 2010)(http://www.molgen.ua.ac.be/admutations) and 11 of the 23 subjects in our initial paper were from families with the A431E *PSEN1* mutation. Though none had SP at the time

of their participation in that study, our results are consistent with the A431E *PSEN1* mutation having a particular effect on white matter integrity which is greatest in association with SP.

Supportive of a direct effect of the A431E *PSEN1* mutations on neuronal projections in the etiology of SP is the finding of delayed SSEPs from the lower extremities in our subject. SSEPs are thought to reflect conduction through the medial lemniscus and therefore our findings are consistent with abnormalities in the projections arising from the dorsal root ganglion or their rostral extension from the nuclei cuneatus and gracilis in the medulla. Though upregulation of APP has been described in the dorsal root ganglion(Nishimura et al, 2003) such conduction abnormalities have not, to our knowledge, been described in LOAD and therefore may represent an effect of the A431E *PSEN1* mutation independent of APP processing. Note that in the one neuropathological report in which the lemniscal pathways were described in a patient with *PSEN1*-related SP, no gross abnormalities were seen(Rudzinski, Fletcher, 2008) and SSEPs were described as being normal in the subject with spastic paraparesis imaged with tau PET in the study of Lyoo et al(Lyoo, Cho, 2016).

Though we found imaging and electrophysiological evidence of widespread white matter abnormalities in *PSEN1* mutation-related SP, there are limitations in our ability to determine the underlying mechanism. Our groups were not as comparable with regards to gender and distribution of *APOE* genotype as would have been ideal. Though all persons with SP were males in this study, we have seen females with the SP associated with the A431E *PSEN1* mutation. In post-hoc analyses we performed comparisons of DTI measures between the 3 males with SP and the two males without. No statistically significant differences were seen in specific anatomical areas. However, mean white matter FA was higher (0.43 vs. 0.38) and MD lower (0.00077 vs. 0.00083) in males without SP than in those with, suggesting the effects seen were more likely to be related to the presence of SP than to gender.

Though all 3 SP subjects in our study had non-ε3/3 *APOE* genotypes, one non-SP subject was of the *APOE* ε4/4 genotype. SP is characteristic of specific *PSEN1* mutations rather than of *PSEN1* mutations in general in the context of a non-*APOE* ε3 allele. Similarly, the overabundance of MCH's (and presumably, CAA) in persons with SP does not easily explain this clinical feature. However, a limitation of our study is that MCH's were quantified from either GRE or SWI images in different subjects, limiting our ability to compare them. Importantly, with the exception of the one sibling with the A431E *PSEN1* mutation without SP, the remaining 6 subjects without SP all had mutations that have not been reported as being associated with SP, enhancing our ability to isolate the effects of a *PSEN1* mutation consistently associated with this atypical feature. In additional post-hoc analyses we compared diffusion measures between the 3 subjects with SP to the one subject with the A431E *PSEN1* mutation but without SP using the approach described above. Though no significant differences were found in specific tracts, average white matter FA was numerically higher (0.42 vs. 0.39) and MD lower (0.00079 vs. 0.00083) in the subject without SP compared to those with SP. This is consistent with the differences seen being more closely related to SP than to the A431E *PSEN1* mutation *per se.* Similar comprehensive evaluations, including identical imaging, electrophysiological and

biochemical assessments, of a larger number of subjects with and without SP and the A431E and other *PSEN1* mutations should help clarify the etiology of SP in this context.

In this study we have documented widespread DTI abnormalities despite relatively preserved gray matter volumes in persons with SP associated with the A431E *PSEN1* mutation. With the single subject with SP that underwent electrophysiological studies and amyloid imaging showing conduction abnormalities in the corticospinal, transcallosal, and lemniscal tracts in the context of insignificant PiB signal in relevant cortical regions, our data support the presence of diffuse white matter abnormalities that may be independent of fibrillar amyloid deposition in the etiology of this unusual clinical feature in persons with the A431E *PSEN1* mutation.

Acknowledgments

References

1. Akoudad S, de Groot M, Koudstaal PJ, van der Lugt A, Niessen WJ, Hofman A, et al. Cerebral microbleeds are related to loss of white matter structural integrity. Neurology. 2013 Nov 26; 81(22): 1930–7. [PubMed: 24174590]

2. Alzheimer's A. 2015 Alzheimer's disease facts and figures. Alzheimers Dement. 2015 Mar; 11(3): 332–84. [PubMed: 25984581]

3. Athan ES, Williamson J, Ciappa A, Santana V, Romas SN, Lee JH, et al. A founder mutation in presenilin 1 causing early-onset Alzheimer disease in unrelated Caribbean Hispanic families. Jama. 2001; 286(18):2257–63. [PubMed: 11710891]

4. Back SA, Kroenke CD, Sherman LS, Lawrence G, Gong X, Taber EN, et al. White matter lesions defined by diffusion tensor imaging in older adults. Ann Neurol. 2011 Sep; 70(3):465–76. [PubMed: 21905080]

5. Bozzali M, Falini A, Franceschi M, Cercignani M, Zuffi M, Scotti G, et al. White matter damage in Alzheimer's disease assessed in vivo using diffusion tensor magnetic resonance imaging. J Neurol Neurosurg Psychiatry. 2002 Jun; 72(6):742–6. [PubMed: 12023417]

6. Clark CM, Schneider JA, Bedell BJ, Beach TG, Bilker WB, Mintun MA, et al. Use of florbetapir-PET for imaging beta-amyloid pathology. Jama. 2011 Jan 19; 305(3):275–83. [PubMed: 21245183]

7. Fazekas F, Chawluk JB, Alavi A, Hurtig HI, Zimmerman RA. MR signal abnormalities at 1.5 T in Alzheimer's dementia and normal aging. AJR Am J Roentgenol. 1987 Aug; 149(2):351–6. [PubMed: 3496763]

8. Folstein MF, Folstein SE, McHugh PR. "Mini-mental state" A practical method for grading the cognitive state of patients for the clinician. J Psychiatr Res. 1975 Nov; 12(3):189–98. [PubMed: 1202204]

9. Gomez-Isla T, Wasco W, Pettingell WP, Gurubhagavatula S, Schmidt SD, Jondro PD, et al. A novel presenilin-1 mutation: increased beta-amyloid and neurofibrillary changes. Ann Neurol. 1997 Jun; 41(6):809–13. [PubMed: 9189043]

10. Hardy J, Selkoe DJ. The amyloid hypothesis of Alzheimer's disease: progress and problems on the road to therapeutics. Science. 2002 Jul 19; 297(5580):353–6. [PubMed: 12130773]

11. Houlden H, Baker M, McGowan E, Lewis P, Hutton M, Crook R, et al. Variant Alzheimer's disease with spastic paraparesis and cotton wool plaques is caused by PS-1 mutations that lead to

exceptionally high amyloid-beta concentrations. Ann Neurol. 2000; 48(5):806–8. [PubMed: 11079548]

12. Joshi A, Ringman JM, Lee AS, Juarez KO, Mendez MF. Comparison of clinical characteristics between familial and non-familial early onset Alzheimer's disease. J Neurol. 2012 Oct; 259(10): 2182–8. [PubMed: 22460587]

13. Karlstrom H, Brooks WS, Kwok JB, Broe GA, Kril JJ, McCann H, et al. Variable phenotype of Alzheimer's disease with spastic paraparesis. J Neurochem. 2008 Feb; 104(3):573–83. [PubMed: 17995932]

14. Klunk WE, Engler H, Nordberg A, Bacskai BJ, Wang Y, Price JC, et al. Imaging the pathology of Alzheimer's disease: amyloid-imaging with positron emission tomography. Neuroimaging Clin N Am. 2003 Nov; 13(4):781–9. ix. [PubMed: 15024961]

15. Koivunen J, Verkkoniemi A, Aalto S, Paetau A, Ahonen JP, Viitanen M, et al. PET amyloid ligand [11C]PIB uptake shows predominantly striatal increase in variant Alzheimer's disease. Brain. 2008 Jul; 131(Pt 7):1845–53. [PubMed: 18583368]

16. Kwok JB, Taddei K, Hallupp M, Fisher C, Brooks WS, Broe GA, et al. Two novel (M233T and R278T) presenilin-1 mutations in early-onset Alzheimer's disease pedigrees and preliminary evidence for association of presenilin-1 mutations with a novel phenotype. Neuroreport. 1997 Apr 14; 8(6):1537–42. [PubMed: 9172170]

17. Larner AJ. Presenilin-1 mutations in Alzheimer's disease: an update on genotype-phenotype relationships. J Alzheimers Dis. 2013; 37(4):653–9. [PubMed: 23948899]

18. Le TV, Crook R, Hardy J, Dickson DW. Cotton wool plaques in non-familial late-onset Alzheimer disease. J Neuropathol Exp Neurol. 2001 Nov; 60(11):1051–61. [PubMed: 11706935]

19. Li X, Westman E, Stahlbom AK, Thordardottir S, Almkvist O, Blennow K, et al. White matter changes in familial Alzheimer's disease. J Intern Med. 2015 Aug; 278(2):211–8. [PubMed: 25639959]

20. Lyoo CH, Cho H, Choi JY, Hwang MS, Hong SK, Kim YJ, et al. Tau Accumulation in Primary Motor Cortex of Variant Alzheimer's Disease with Spastic Paraparesis. J Alzheimers Dis. 2016 Feb 16; 51(3):671–5. [PubMed: 26890779]

21. Llado A, Fortea J, Ojea T, Bosch B, Sanz P, Valls-Sole J, et al. A novel PSEN1 mutation (K239N) associated with Alzheimer's disease with wide range age of onset and slow progression. Eur J Neurol. 2010 Jul; 17(7):994–6. [PubMed: 20158511]

22. Martikainen P, Pikkarainen M, Pontynen K, Hiltunen M, Lehtovirta M, Tuisku S, et al. Brain pathology in three subjects from the same pedigree with presenilin-1 (PSEN1) P264L mutation. Neuropathol Appl Neurobiol. 2010 Feb; 36(1):41–54. [PubMed: 19849793]

23. Medina D, DeToledo-Morrell L, Urresta F, Gabrieli JD, Moseley M, Fleischman D, et al. White matter changes in mild cognitive impairment and AD: A diffusion tensor imaging study. Neurobiol Aging. 2006 May; 27(5):663–72. [PubMed: 16005548]

24. Miller JA, Oldham MC, Geschwind DH. A systems level analysis of transcriptional changes in Alzheimer's disease and normal aging. J Neurosci. 2008 Feb 6; 28(6):1410–20. [PubMed: 18256261]

25. Miravalle L, Calero M, Takao M, Roher AE, Ghetti B, Vidal R. Amino-terminally truncated Abeta peptide species are the main component of cotton wool plaques. Biochemistry. 2005 Aug 16; 44(32):10810–21. [PubMed: 16086583]

26. Morelli L, Prat MI, Levy E, Mangone CA, Castano EM. Presenilin 1 Met146Leu variant due to an A --> T transversion in an early-onset familial Alzheimer's disease pedigree from Argentina. Clin Genet. 1998 Jun; 53(6):469–73. [PubMed: 9712537]

27. Morris JC. Clinical dementia rating: a reliable and valid diagnostic and staging measure for dementia of the Alzheimer type. Int Psychogeriatr. 1997; 9(Suppl 1):173–6. discussion 7–8. [PubMed: 9447441]

28. Murrell J, Ghetti B, Cochran E, Macias-Islas MA, Medina L, Varpetian A, et al. The A431E mutation in PSEN1 causing familial Alzheimer's disease originating in Jalisco State, Mexico: an additional fifteen families. Neurogenetics. 2006 Nov; 7(4):277–9. [PubMed: 16897084]

29. Nishimura I, Takazaki R, Kuwako K, Enokido Y, Yoshikawa K. Upregulation and antiapoptotic role of endogenous Alzheimer amyloid precursor protein in dorsal root ganglion neurons. Exp Cell Res. 2003 Jun 10; 286(2):241–51. [PubMed: 12749853]

30. O'Riordan S, McMonagle P, Janssen JC, Fox NC, Farrell M, Collinge J, et al. Presenilin-1 mutation (E280G), spastic paraparesis, and cranial MRI white-matter abnormalities. Neurology. 2002 Oct 8; 59(7):1108–10. [PubMed: 12370477]

31. Pigino G, Morfini G, Pelsman A, Mattson MP, Brady ST, Busciglio J. Alzheimer's presenilin 1 mutations impair kinesin-based axonal transport. J Neurosci. 2003 Jun 1; 23(11):4499–508. [PubMed: 12805290]

32. Ringman JM, Gylys KH, Medina LD, Fox M, Kepe V, Flores DL, et al. Biochemical, neuropathological, and neuroimaging characteristics of early-onset Alzheimer's disease due to a novel PSEN1 mutation. Neurosci Lett. 2011 Jan 10; 487(3):287–92. [PubMed: 21094210]

33. Ringman JM, Liang LJ, Zhou Y, Vangala S, Teng E, Kremen S, et al. Early behavioural changes in familial Alzheimer's disease in the Dominantly Inherited Alzheimer Network. Brain. 2015 Apr; 138(Pt 4):1036–45. [PubMed: 25688083]

34. Ringman JM, Monsell S, Ng DW, Zhou Y, Nguyen A, Coppola G, et al. Neuropathology of Autosomal Dominant Alzheimer Disease in the National Alzheimer Coordinating Center Database. J Neuropathol Exp Neurol. 2016 Feb 17.

35. Ringman JM, O'Neill J, Geschwind D, Medina L, Apostolova LG, Rodriguez Y, et al. Diffusion tensor imaging in preclinical and presymptomatic carriers of familial Alzheimer's disease mutations. Brain. 2007 Jul; 130(Pt 7):1767–76. [PubMed: 17522104]

36. Ringman JM, Teplow DB, Villemagne VL. The exception makes the rule: not all Abeta plaques are created equal. Neurology. 2012 Jul 17; 79(3):206–7. [PubMed: 22700807]

37. Ringman JM, Younkin SG, Pratico D, Seltzer W, Cole GM, Geschwind DH, et al. Biochemical markers in persons with preclinical familial Alzheimer disease. Neurology. 2008 Jul 8; 71(2):85–92. [PubMed: 18509095]

38. Roher AE, Maarouf CL, Malek-Ahmadi M, Wilson J, Kokjohn TA, Daugs ID, et al. Subjects harboring presenilin familial Alzheimer's disease mutations exhibit diverse white matter biochemistry alterations. Am J Neurodegener Dis. 2013; 2(3):187–207. [PubMed: 24093083]

39. Rudzinski LA, Fletcher RM, Dickson DW, Crook R, Hutton ML, Adamson J, et al. Early onset familial Alzheimer Disease with spastic paraparesis, dysarthria, and seizures and N135S mutation in PSEN1. Alzheimer Dis Assoc Disord. 2008 Jul-Sep;22(3):299–307. [PubMed: 18580586]

40. Ryan NS, Keihaninejad S, Shakespeare TJ, Lehmann M, Crutch SJ, Malone IB, et al. Magnetic resonance imaging evidence for presymptomatic change in thalamus and caudate in familial Alzheimer's disease. Brain. 2013 May; 136(Pt 5):1399–414. [PubMed: 23539189]

41. Sanchez-Valle R, Monte GC, Sala-Llonch R, Bosch B, Fortea J, Llado A, et al. White Matter Abnormalities Track Disease Progression in PSEN1 Autosomal Dominant Alzheimer's Disease. J Alzheimers Dis. 2016 Feb 20; 51(3):827–35. [PubMed: 26923015]

42. Scheuner D, Eckman C, Jensen M, Song X, Citron M, Suzuki N, et al. Secreted amyloid beta-protein similar to that in the senile plaques of Alzheimer's disease is increased in vivo by the presenilin 1 and 2 and APP mutations linked to familial Alzheimer's disease. Nat Med. 1996 Aug; 2(8):864–70. [PubMed: 8705854]

43. Shrimpton AE, Schelper RL, Linke RP, Hardy J, Crook R, Dickson DW, et al. A presenilin 1 mutation (L420R) in a family with early onset Alzheimer disease, seizures and cotton wool plaques, but not spastic paraparesis. Neuropathology. 2007 Jun; 27(3):228–32. [PubMed: 17645236]

44. Song SK, Sun SW, Ju WK, Lin SJ, Cross AH, Neufeld AH. Diffusion tensor imaging detects and differentiates axon and myelin degeneration in mouse optic nerve after retinal ischemia. Neuroimage. 2003 Nov; 20(3):1714–22. [PubMed: 14642481]

45. Song SK, Sun SW, Ramsbottom MJ, Chang C, Russell J, Cross AH. Dysmyelination revealed through MRI as increased radial (but unchanged axial) diffusion of water. Neuroimage. 2002 Nov; 17(3):1429–36. [PubMed: 12414282]

46. Sun X, Salat D, Upchurch K, Deason R, Kowall N, Budson A, et al. Destruction of white matter integrity in patients with mild cognitive impairment and Alzheimer disease. J Investig Med. 2014 Oct; 62(7):927–33.

47. Tanzi RE, Moir RD, Wagner SL. Clearance of Alzheimer's Abeta peptide: the many roads to perdition. Neuron. 2004 Sep 2; 43(5):605–8. [PubMed: 15339642]

48. Ting SK, Benzinger T, Kepe V, Fagan A, Coppola G, Porter V, et al. A novel PSEN1 mutation (I238M) associated with early-onset Alzheimer's disease in an African-American woman. J Alzheimers Dis. 2014; 40(2):271–5. [PubMed: 24413619]

49. Torosyan N, Silverman DH. Neuronuclear imaging in the evaluation of dementia and mild decline in cognition. Semin Nucl Med. 2012 Nov; 42(6):415–22. [PubMed: 23026363]

50. Verkkoniemi A, Kalimo H, Paetau A, Somer M, Iwatsubo T, Hardy J, et al. Variant Alzheimer disease with spastic paraparesis: neuropathological phenotype. J Neuropathol Exp Neurol. 2001 May; 60(5):483–92. [PubMed: 11379823]

51. Wirths O, Weis J, Szczygielski J, Multhaup G, Bayer TA. Axonopathy in an APP/PS1 transgenic mouse model of Alzheimer's disease. Acta Neuropathol (Berl). 2006 Apr; 111(4):312–9. [PubMed: 16520967]

52. Xia D, Watanabe H, Wu B, Lee SH, Li Y, Tsvetkov E, et al. Presenilin-1 Knockin Mice Reveal Loss-of-Function Mechanism for Familial Alzheimer's Disease. Neuron. 2015 Mar 4; 85(5):967–81. [PubMed: 25741723]

53. Yescas P, Huertas-Vazquez A, Villarreal-Molina MT, Rasmussen A, Tusie-Luna MT, Lopez M, et al. Founder effect for the Ala431Glu mutation of the presenilin 1 gene causing early-onset Alzheimer's disease in Mexican families. Neurogenetics. 2006 Jul; 7(3):195–200. [PubMed: 16628450]

54. Yokota O, Terada S, Ishizu H, Ujike H, Ishihara T, Namba M, et al. Variability and heterogeneity in Alzheimer's disease with cotton wool plaques: a clinicopathological study of four autopsy cases. Acta Neuropathol. 2003 Oct; 106(4):348–56. [PubMed: 12883830]

Author Manuscript

Author Manuscript

Author Manuscript

Author Manuscript

Highlights

Highlights of the current paper are:

1. We found widespread abnormalities of white matter using DTI in persons with PSEN1-spastic paraparesis that were not confined to the corticospinal tract, relative to persons with PSEN1 mutations without spastic paraparesis.

2. There was a relative paucity of amyloid signal in the cortex of a subject with spastic paraparesis and clearly not increased signal in the sensorimotor cortex.

3. Electrophysiological studies confirmed slowed motor evoked potentials to the legs and suggested slowed somatosensory conduction from the legs as well, suggesting widespread white matter abnormalities.

In aggregate these data suggest that spastic paraparesis in PSEN1-related AD is but one sign of widespread abnormalities of white matter that may arise independently of aberrant Abeta metabolism.
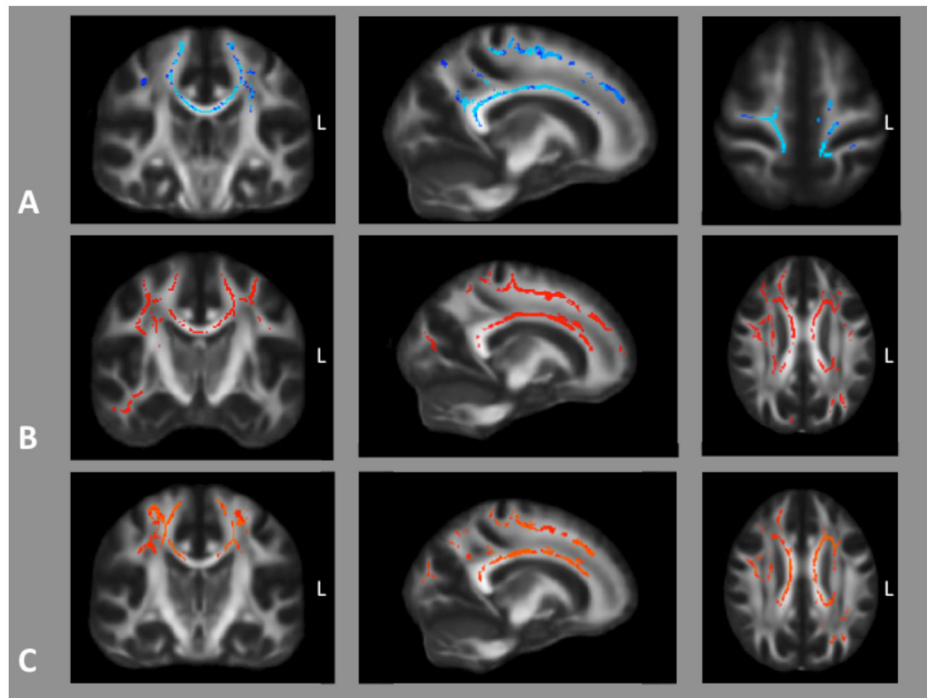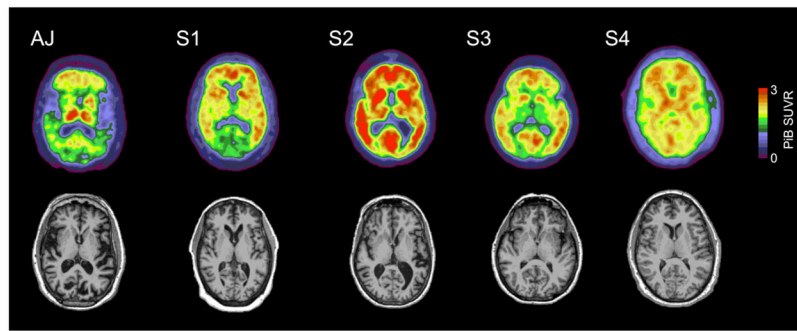
Figure 1.
A) Voxels in which fractional anisotropy was significantly lower (p < 0.05, FDR corrected) in 3 subjects with *PSEN1*-related SP relative to 7 without. B) Voxels in which MD was higher and C) radial diffusivity higher in subjects with SP. There were no areas were axial diffusivity differed between groups.
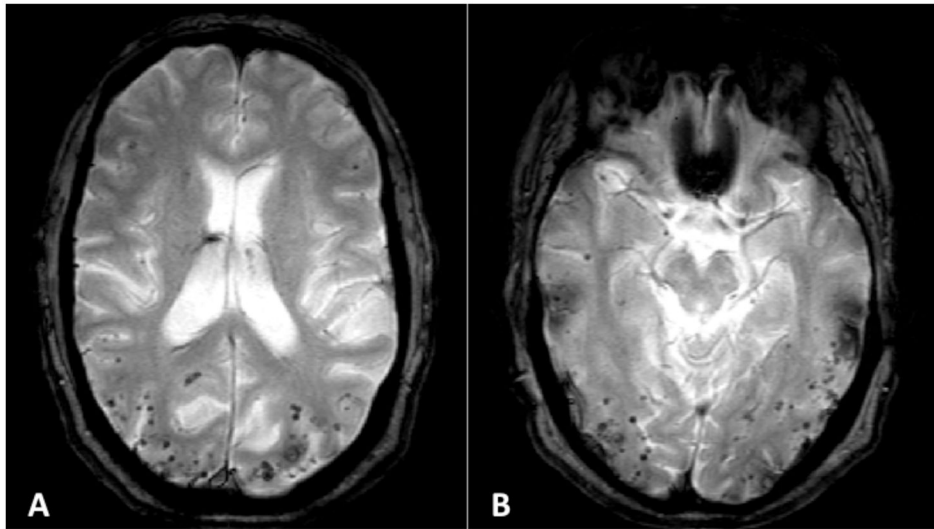
Figure 2.
Extensive lobar microhemorrhages seen on susceptibility-weighted MRI in "AJ" a 49 year-old man carrying the A431E *PSEN1* mutation with spastic paraparesis. Note the predilection for the parietal and occipital lobes.

Figure 3.
PiB images in a subject with SP due to the A431E *PSEN1* mutation ("AJ") and four without SP. Note the overall reduced PiB signal in AJ except for relatively selective deposition in the thalamus.

Table 1

Demographic, clinical, and genetic characteristics of the study population. P-values denote significance for Mann-Whitney U tests, Chi-Square tests, and Fisher's exact tests as appropriate.

	PSEN1 **mutation carriers with SP (n = 3)**	*PSEN1* **mutation carriers without SP (n = 7)**	
Mean age in years (s.d.)	48.7 (1.5)	54.7 (8.6)	p = 0.38
Mean duration of cognitive and/or motor symptoms in years (s.d.)	5.3 (2.5)	5.3 (6.0)	p = 0.52
Mean years after age of median family-specific age of dementia diagnosis (s.d.)	0.0 (5.7)	2.7 (6.4)	p = 0.53
Gender, # female (%female)	0 (0%)	5 (71%)	p = 0.17
APOE genotype distribution	3/4 (n = 2), 2/3 (n = 1)	3/3 (n = 6), 4/4 (n = 1)	***p = 0.02***
Specific mutations	A431E (all 3)	A431E (n =1), G206A (n = 2), I238M, M146L, R269H, S212Y (each = 1)	p = 0.27
Mean MMSE (s.d.)	15.3 (10.4)	18.0 (10.7)	p = 0.67
Mean CDR total scores	0.5 (n= 2), 3 (n = 1)	0.5 (n = 3), 1 (n = 2), 2 (n = 1), 3 (n = 1)	p = 0.83
Mean CDR sum of boxes (s.d.)	6.7 (7.2)	6.9 (6.5)	p = 0.83

Table 2

Quantitative imaging variables compared between symptomatic *PSEN1* mutation carriers with and without SP by two-sided t-tests. *Microhemorrhage counts greater than 100 were quantified as 100. Comparisons were made using Mann-Whitney U tests.

	PSEN1 mutation carriers with SP (n = 3)	*PSEN1* mutation carriers without SP (n = 7)	
Mean cerebellar volume mm^3 (s.d.)	122,053 (4,708)	128,625 (17,892)	p = 1.00
Mean caudate volume mm^3 (s.d.)	6,389 (784)	6,854 (620)	p = 0.38
Mean putamen volume mm^3 (s.d.)	8,617 (1,534)	9,248 (1128)	p = 0.67
Mean pallidum volume mm^3 (s.d.)	2,908 (124)	3,116 (218)	p = 0.27
Mean amygdala volume mm^3 (s.d.)	2,787 (672)	2,598 (652)	p = 0.83
Mean right hippocampal volume mm^3 (s.d.)	2,982 (331)	3,146 (720)	p = 0.67
Mean left hippocampal volume mm^3 (s.d.)	3,000 (215)	3,112 (639)	p = 0.83
Mean occipital cortex thickness mm (s.d.)	1.72 (0.05)	1.90 (0.15)	p = 0.12
Mean temporal cortex thickness mm (s.d.)	2.66 (0.33)	2.83 (0.16)	p = 0.38
Mean parietal cortex thickness mm (s.d.)	2.05 (0.06)	2.18 (0.22)	p = 0.67
Mean frontal cortex thickness mm (s.d.)	2.39 (0.11)	2.44 (0.09)	p = 0.67
Mean WMH volume – mm^3 (s.d.)	17,978 (3,651)	9,491 (15,954) (n = 5)	p = 0.25
Mean Fazekas score (s.d.)	2.0 (1.0)	1.2 (1.3) (n = 5)	p = 0.39
# microhemorrhages*	66.7 (57.7)	12.2 (29.8) (n = 6)	p = 0.17

Table 3

SUVRs for various cerebral regions in one carrier of the A431E *PSEN1* mutation with SP relative to 4 *PSEN1* mutation carriers without SP.

	Subject with spastic paraparesis (AJ)	4 subjects without spastic paraparesis
Mean cortical binding potential	0.21	0.84 (0.42)
Mean left posterior cingulate cortex (s.d.)	1.46	2.57 (0.72)
Mean right posterior cingulate cortex (s.d.)	1.58	2.36 (0.76)
Mean left primary visual cortex (s.d.)	1.52	2.20 (0.73)
Mean right primary visual cortex (s.d.)	1.50	2.06 (0.59)
Mean left sensorimotor cortex (s.d.)	1.06	1.97 (0.30)
Mean right sensorimotor cortex (s.d.)	1.15	1.99 (0.34)
Mean left thalamus (s.d.)	1.72	1.93 (0.65)
Mean right thalamus (s.d.)	1.86	2.00 (0.49)
Mean left caudate nucleus (s.d.)	1.21	2.02 (0.65)
Mean right caudate nucleus (s.d.)	1.08	2.07 (0.52)
Mean reft cerebellum (s.d.)	1.00	1.02 (0.00)
Mean right cerebellum (s.d.)	0.99	0.98 (0.00)